miR-466 Regulates the Migration of ADSCs in Repairing Cutaneous Wound via Targeting SCF/c-kit/ERK Signaling Axis

sizhan xia
Zhejiang University School of Medicine Second Affiliated Hospital
wei zhang
Zhejiang University School of Medicine Second Affiliated Hospital
ronghua jin
Zhejiang University School of Medicine Second Affiliated Hospital
tingting weng
Zhejiang University School of Medicine Second Affiliated Hospital
meirong yu
Zhejiang University School of Medicine Second Affiliated Hospital
min yang
Zhejiang University School of Medicine Second Affiliated Hospital
jiaming shao
Zhejiang University School of Medicine Second Affiliated Hospital
xingang wang
Zhejiang University School of Medicine Second Affiliated Hospital
chunmao han (zrssk@zju.edu.cn)
Zhejiang University

Research

Keywords: adipose-derived stem cells, miR-466, stem cell factor, wound healing

Posted Date: March 16th, 2021

DOI: https://doi.org/10.21203/rs.3.rs-293054/v1

Abstract

Background

Wound healing is a complex process and the treatment of chronic non-healing wounds still remains a tough challenge. Mesenchymal stem cell (MSC) based therapy has emerged as a promising therapeutic strategy for wound healing. Stem cell factor/stem cell factor receptor (SCF/c-kit) interaction activates downstream signal pathways in stem cells. microRNAs (miRNAs) regulate the effect of adipose tissue-derived stem cells (ADSCs) in cutaneous wound, but the associated cellular mechanisms are not fully understood. In the research, we investigate the inhibitory effect of miR-466 in ADSC migration induced by SCF/c-kit/ERK axis.

Methods

Human ADSCs were tested by scratch assay and Transwell assay to evaluate the migration ability. MicroRNA sequencing was used to find the discrepancy miRNA in ADSCs with or without SCF pretreatment. The ERK signaling pathway was investigated by pharmacological disruption of PD98059. In addition, siRNA, RT-qPCR, western blotting, and luciferase reporter assay were used to investigate the mechanism of miR-466 regulating migration via the SCF/c-kit/ERK pathway. In the in vivo study, the wound healing ability of miR-466 and SCF was evaluated in a nude mouse full-thickness skin wound model.

Results

ADSCs incubated with SCF induces the expression of c-kit and promotes ADSC migration, whereas siRNA c-kit inhibited the effects. microRNAs microarray showed that miR-466 was upregulated in SCF pretreatment ADSCs compared to ADSCs. The luciferase reporter assay indicated that miR-466 may target c-kit and suppress SCF/c-kit-mediated migration of ADSCs. The ERK signaling pathway was confirmed to be involved in SCF/c-kit induced migration. In addition, pre-treatment with PD98059 reversed the effects of SCF/c-kit on the ERK signaling and migration-related proteins. Furthermore, miR-466 inhibits ADSC migration to wound site and defects cutaneous wound healing in vivo.

Conclusions

Taken together, our data suggested that SCF/c-kit signal axis can enhance the activation of ERK signal pathway, which will promote ADSC migration. miR-466 regulates ADSC migration by targeting SCF/c-kit/ERK signaling and defects wound healing.

Introduction

Originally derived from mesoblast, adipose tissue-derived stem cells (ADSCs) are easily accessible with minimal invasiveness, which harbor the ability of self-renewal and multilineage potential, differentiating into keratinocytes, fibroblasts, and angiogenic cells [1, 2]. A large number of studies have indicated that

implantation of ADSCs shows promising properties in wound healing [3–5]. During wound healing, ADSCs show a great ability in migration to be recruited rapidly into the wound site, providing the potentially influent for a faster wound healing response [6]. But the harsh microenvironment of the damaged cutaneous tissue expresses high levels of oxidative stress, hypoxia, advanced glycation end products (AGEs) or inflammation, which decreases cellular activity and inhibits migrating of ADSCs to wound site, thus impedes wound healing [7–9]. Therefore, it is necessary to understand the intervention mechanisms that improve the vitality of seed cells more simply and efficiently during wound healing, which may provide new insights into chronic wound treatment.

Stem cell factor (SCF), also called c-kit ligand, steel factor, and mast cell growth factor, is composed of 164 amino acids and has a molecular weight of 30 kDa [10, 11]. It provides the bridge between intracellular and extracellular function through the specific receptor for c-kit. After c-kit binding to its ligand in the extracellular ligand binding region, the structure of c-kit monomer changes, resulting in homopolymerization, which leads to automatic phosphorylation of amino, initiation of SCF/c-kit signaling pathway, and mediating various secondary signaling molecules to regulate cell functions [12, 13]. SCF/c-kit interaction regulates the mobilization and recruitment of stem cells, including hemopoietic stem cells, cardiac stem cell, BMSCs and utero–labeled stem cells [14, 15]. Numerous of articles have documented that SCF can improve the survival ability of cells and inhibit apoptosis [16, 17]. The interaction between c-kit and SCF plays an important role in proliferation and migration of stem cells and leads to a diverse array of signaling pathways activation, such as p38 and ERK that participate in migration [18, 19].

miRNAs are ubiquitously expressed a class of non-coding single-stranded small molecular RNA with a length of about 18–25 nucleotides, which can be complementary paired with the 3'-UTR of messenger RNAs (mRNAs), thus leading to degradation of the target mRNAs and/or translation inhibition [20]. miRNAs act regulatory effects in cell proliferation, differentiation, apoptosis and metabolism [21, 22]. Recently, several miRNAs have been demonstrated to interfere with and modulate intracellular signal transduction related to wound healing [23, 24]. However, few studies explore the role of miRNAs in SCF/c-kit signaling related to wound healing. In this study, we focused on miR-466 via a microRNA array after ADSCs exposure to SCF. Then, we focused on the role of miR-466 in ADSCs exposed to SCF, and found that miR-466 regulated the effect of ADSCs in repairing wound healing via targeting SCF/c-kit/ERK signaling axis.

Materials And Methods

Isolation and Culture of Human ADSCs

Human ADSCs were isolated from subcutaneous adipose tissue which obtained from patients (age range 30–45 years) undergoing cosmetic liposuction. All of donors gave written informed consents. Then, minced tissues were digested with 0.1% collagenase I (Invitrogen-Gibco, Carlsbad, CA, USA) and incubated for 45 min at 37°C. After enzymatic digestion, centrifuged and filtered cell pellet was collected

and cultured in L-Dulbecco's modified Eagle's medium/F12 (DMEM/F12; Invitrogen Life Technologies, Carlsbad, CA, USA) plus 10% fetal bovine serum (FBS; Invitrogen Life Technologies). Cells were cultured at 37 ˚C and 5% CO_2.

Cell treatment

SCF were obtained from Sigma-Aldrich (St. Louis, MO, USA). SCF were added to ADSCs and then subject to some experiments. Also, a ERK inhibitor, PD98059 (30 μmol/L, Beyotime, Shanghai, China) was added to cultured cells to block the ERK activity in this study.

Western blot

Total protein was extracted from treated cells lysed in radio immunoprecipitation assay (RIPA) buffer and protein concentration was quantified using a BCA protein assay kit. Proteins were separated on 10% or 12% sodium dodecyl sulfate polyacrylamide gel, then transferred to a nitrocellulose membrane and incubated overnight at 4˚C with the primary antibodies. After three washes with TBS plus 0.1% Tween-20 (TBST), Membranes were incubated with the following antibodies: rabbit polyclonal against c-kit (1:500; Abcam, CA, USA), MMP-2 (1:500; Abcam), MMP-9 (1:500; Abcam), JNK (1:500, Cell Signaling Technology, MA, USA), p-JNK (1:500, Cell Signaling Technology) and rabbit monoclonal against β-actin (1:1000; Cell Signaling Technology). Immunoreactive protein bands were detected with BD scanning system.

Cell transfection

The c-kit siRNAs, miR-466 mimics and inhibitor were purchased from GenePharma (Shanghai, China). The sequences for the c-kit siRNA and miR-466 used for the experiments were as follows:

c-kit siRNA1: 5'-CCGUGACAUUCAACGUUUATT-3'

c-kit siRNA2: 5'-CGAUCCGGAGCUGCGCCUATT-3'

miR-466 mimic: 5'-AUACACAUACACGCAACACACAU-3'

miR-466 mimic NC: 5'-UUCUCCGAACGUGUCACGUTT-3'

miR-466 inhibitor: 5'-AUGUGUGUUGCGUGUAUGUGUAU-3'

miR-466 inhibitor NC: 5'-CAGUACUUUUGUGUAGUACAA-3'

ADSCs were plated in 6-well or 96-well plates and transient transfection using Lipofectamine^{TM}3000 (Invitrogen, CA, USA) according to the manufacturer’s instructions.

RNA extraction and quantitative PCR (qPCR)

Total RNA extraction from ADSCs was performed with Trizol™ (Invitrogen), according to the manufacturer's instructions. cDNA was transcribed reversely according to the manufacturer’s instructions of PrimeScript RT-PCR kit (Takara, Japan) from total RNA extracted from treated cells with Trizol

(Invitrogen, USA). RT-qPCR was performed on a 7500HT Fast RT-PCR instrument using SYBR-Green. The PCR parameters for relative quantification were as follows: 2 min at 95°C, followed by 40 cycles of 45 sec at 57°C and 45 sec at 72°C. The relative expression was evaluated following the relative quantification equation, $2^{-\Delta\Delta CT}$. The primers were designed as follows: miR-466, forward 5'-ATGGTTCGTGGGATACACATACACGCA-3', reverse 5'-GCAGGGTCCGAGGTATTC-3'; U6, forward 5'-GCTTCGGCAGCACATATACTA

AAAT-3', reverse 5'-CGCTTCACGAATTTGCGTGTCAT-3'; c-kit, forward 5'-CACCGAAGGAGGCACTTACAC-3', reverse 5'-ACACACCGTCGTCCGAAGG-3';

GAPDH, forward, 5’-CTGGGCTACACTGAGCACC-3’, reverse5’- AAGTGGTCGT

TGAGGGCAATG – 3’. GAPDH or U6 was used as an internal control.

Cell scratch assay

Cells were cultured in 6-well plates overnight. Cells at passages 4–6 were used in this study. After reaching confluence, a scratch was performed on the cell monolayer using a 200 μL pipette tip, resembling an artificial in vitro wound. The drifting cells were washed away and removed by PBS. After the cells were supplemented with fresh medium, the wound healing was observed and photographed at 24 h after the injury. The wound-healing rate was quantitatively evaluated using the Image J software.

Transwell migration assay

Cell migration was determined by using transwell chambers with a pore size of 8 μm. In migration assay, 2×10^4 ADSCs were seeded in the upper chamber resuspend with serum-free medium. After 48 h of incubation, discarded cells and supernant on the upper half of the membrane, and cells on the lower surface of the membrane were fixed with methanol and stained with leucocrystal violet. The cells were counted in three random fields under a light microscope. All assays were carried out in triplicate.

microRNAs microarray

The high-throughput sequencing service and subsequent bioinformatics analysis were provided by Lianchuan Biotech (Hangzhou, China). Briefly, Total RNA extraction from ADSCs was performed with Trizol™ (Invitrogen), according to the manufacturer's instructions. The lab procedures followed Illumina's standard procedures, including preparation of libraries and sequencing experiments. The Small RNA sequencing library was prepared using TruSeq Small RNA Sample Prep Kits (Illumina, San Diego, USA). After the preparation of the library was completed, the constructed library was sequenced by Illumina HiSeq2000/2500, and the sequencing read length was 1×50bp on a single end. Then, clean reads were obtained after quality control processing. Clean reads removed the 3 connectors, and length screening was performed to retain the sequence with base length of 18-26nt.Then, the remaining sequences were compared with RNA database sequences (excluding miRNA), such as mRNA database, RFAM, Repbase (repeat sequence database), and filtered. Finally, the obtained data were valid, which could be used for

subsequent analysis of small RNA data. Gene Ontology (GO) and KEGG pathway analyses were based on NCBI.

Bioinformatics analyses

Protein–Protein Interaction (PPI) network represents the c-kit or ERK process by using the public PPI repository STRING v.11.0 (https://www.string-db.org/) [25].

Luciferase reporter gene assay

Putative binding sites of miR-466 were predicted from some Bioinformatics prediction websites like TargetScan (http://www.targetscan.org) and miRbase (http://www.mirdb.org). Wild or mutant type luciferase reporter vector were obtained when GP-miRGLO was inserted with wild or mutant putative binding sites of miR-466. ADSCs (2×10^4) were plated in 48-well plates and co-transfected with GP-miRGLO-c-Kit wild or mutant type luciferase reporter vector and miR-466 mimics or control using lipofectamine 3000 (Invitrogen, USA). After 24 h post-transfection, cells were subjected to the assay with Dual-Luciferase Reporter assay kit (Promega, USA). In summary, cells were collected, washed, and later resuspended with passive lysis buffer to extract protein, similar to what we have done in western blot experiment. Total protein 30 μl/well were added into 48-well plates and renilla luciferase was the standard.

Wound model

Twenty 6-week-old nu/nu athymic nude mice were purchased from the Experimental Animal Center of Zhejiang University and maintained under specific pathogen-free conditions.

All animal studies were approved by Animal Care and Use Committee.
Specifically, excisional wounds were made in the dorsal skin of four groups of nude mice (N = 5) under ketamine anesthesia with a 15 mm biopsy punch. A silicon ring is sutured around the wound to limit the closure of the wound due to skin contraction. The mice received intradermal injection of ADSCS, SCF-ADSCs, PD98059-SCF-ADSCs, or agomiR-SCF-ADSCs immediately after surgery. miR-466 agomiR (500 μl of 1 nM agomiR solution in PBS) was injected intradermally into the wound edges immediately and on 5, 10, and 15 days after wounding. The wounds were recorded with a digital camera. The sequences for the ago miR-466 used for the animal experiments were as follows. agomiR miR-466: 5'-AUACACAUACACGCAACACACAU-3'.

ADSCs survival assay in vivo

ADSCs were marked with 1,1’-dioctadecyl-3,3,3’,3’-tetramethylindotricarbocyanine (DiR) prior to injection. Five groups of ADSCs were incubated with 3μg/ml DiR at 37°C for 30 min and then washed with PBS for three times. The efficiency of the DiR staining was detected with a fluorescence microscope. Following treatment, $1x10^6$ ADSCs were injected around the wound bed. At 0 day, 3 day, 7 day, 14 day, and 21 day, after transplantation, under isoflurane anesthesia the in vivo imaging system (IVIS) was performed on mice to detect ADSCs.

Histological staining

The skin samples were fixed with 4% paraformaldehyde for 48 h, embedded in paraffin, and cut into 5 μm thick tissue sections. Paraffin sections were heated at 57°C for 60 minutes, deparaffinized and rehydrated, which were used for hematoxylin and eosin (H&E) and Sirius Red according to the manufacturer's manual. Re-epithelialization was calculated according to the following formula: [distance of the minor axis covered by the epithelium]/ [distance of the minor axis between the edges of the original wound] ×100% [26]. The amount of organized collagen tissue was observed on the same cross section with polarized light microscope. Collagen quantification was performed by ImageJ software.

Immunofluorescence staining

For immunofluorescence staining, the tissue sections were deparaffinized, rehydrated, and then incubated with 3% H_2O_2 for 20 min, and the antigen was restored by heating in citrate buffer (pH 6.0). Then the sections were permeabilized and blocked with 1% BSA for 1 h. And the primary antibody solutions were incubated for 16 h at 4 ℃ with the following antibodies: rabbit polyclonal against Keratin10 (1:500; Abcam, CA, USA), CD-31 (1:500; Abcam, CA, USA) and mouse polyclonal against α smooth muscle actin (α-SMA). Subsequently, the tissue sections were incubated with secondary antibody for 1 h at RT in the dark: goat anti-rat IgG Alexa Fluor 488 (1:200, Boster), rat anti-mouse IgG Alexa Fluor 594 (1:200, Boster). Hoechst 33342 (1:10000) was used for the nuclear counterstaining. Fluorescent microscope was used to view the sliders and take photographs. Images were merged and/or quantified using ImageJ.

Statistical analysis

Results were presented as mean ± S.D. and statistically analyzed utilizing a Student's t-test with SPSS software (SPSS 20.0, Inc., Chicago, IL, USA). $P < 0.05$ was considered as a statistically significant difference.

Results

SCF induces c-kit expression, scratch wound closure and cell migration in ADSCs.

The cellular effects of SCF are mainly mediated through the receptor of c-kit. To investigate whether SCF affect the expression of c-kit in ADSCs, cells were incubated with or without SCF (4–48 μg/ml) for 24 h, the expression of c-kit was established by Western blot and RT-qPCR. As shown in Fig. 1A and B, the up-regulation of c-kit in response to SCF was identified in a dose-dependent manner. Scratch closure and transwell assays showed that cell migration was accelerated after SCF treatment (Fig. 1C, D). MMPs are responsible for the higher cell motility and MMP-2 and MMP-9 are known as major chemokine regulators. Consequently, we examined the activity of MMP-2 and MMP-9. Western blot analysis indicated that SCF treatment promoted MMP-2 and MMP-9 activity (Fig. 1E).

Moreover, expression of c-kit in ADSCs following treatment with 32 μg/ml SCF was performed at the different time points. Our results showed a significant increase of c-kit from 0 h to 24 h (Fig. 2A, B). At the

same time, Scratch closure and transwell assays showed that cell migration was accelerated after SCF treatment from 0 h to 24 h in Fig. 2C, D. The up-regulation of MMP-2 and MMP-9 in response to SCF was also shown in a time-dependent manner (Fig. 2E). In conclusion, the results of these functional assays indicate that SCF treatment increases cell migration and accelerates in vitro ADSC scratch closure.

SCF/c-kit axis induces scratch wound closure and cell migration in ADSCs

SCF is involved in regulating the activation and transmission of various signals. To investigate whether c-kit is essential for the role of SCF in ADSCs, we first detected c-kit protein and mRNA levels after using siRNAs for c-kit. The data showed that c-kit was enhanced after exposure to SCF, but declined significantly after transfected with siRNAs for c-kit (Fig. 3A, B). Scratch closure and transwell assays showed that cell migration was increased after SCF treatment, but diminished after knockdown of c-kit (Fig. 3C, D). Western blot assay indicated that siRNAs for c-kit prevented MMP-2 and MMP-9 expression (Fig. 3E). The results of these functional assays reveal that SCF/c-kit axis increases cell migration and accelerates scratch closure.

c-kit is a direct target of miR-466

It has previously been shown that microRNAs efficiently regulate multiple cell functions involved in wound healing. Thus, we used a miRNA array to analyze the miRNA profiles in SCF treated ADSCs and non-treated ADSCs. The results showed that the expression spectrum was different in SCF pretreatment and some miRNAs were upregulated (Fig. 4A). We combined miRDB and Targetscan databases to analyze these up-regulated miRNAs might bind to c-kit. miR-466 was found to be partially complementary to the conserved site in the 3’-UTR of c-kit (Fig. 4B). To determine whether miR-466 binds directly to the 3’-UTR of c-kit to affect its expression, the wild c-kit 3’-UTR (WT) and the mutated (MUT) c-kit 3’UTR were reconstituted into the GP-miRGLO vector. The data showed that introduction of miR-466 diminished luciferase activity of WT 3’-UTR reporter. However, the MUT c-kit 3’-UTR did not

change significantly (Fig. 4C, D). The alignment of c-kit-miR-466 WT/Mut (Fig. 4E).

miR-466 suppresses SCF/c-kit axis-mediated scratch wound closure and cell migration in ADSCs

To further validate whether miR-466 directly targets c-kit, we evaluated the role of miR-466 in the c-kit expression. As shown in Fig. 5A and B, we found that miR-466 mimic reduced c-kit mRNA and protein expression levels in ADSCs. Whereas, miR-466 inhibitor increased c-kit mRNA and protein expression levels in ADSCs (Fig. 4F, G). Taken together, these results indicate that c-kit is a target gene of miR-466. Furthermore,to determine whether miR-466 mediates the role of SCF/c-kit axis in ADSCs migration. Scratch closure and transwell assays showed that miR-466 mimic reduced cell migration which was induced by SCF (Fig. 5B, D). In addition, Western blot analysis for MMP-2 and MMP-9 suggested that

transfected miR-466 mimic inhibited MMP-2 and MMP-9 activity (Fig. 5E). On the contrary, miR-466 inhibitor promoted cell migration induced by SCF (Fig. 5H, I). The activity of MMP-2 and MMP-9 was elevated by miR-466 inhibitor (Fig. 5J).

Activating ERK/MARK signal is involved in SCF/c-kit regulated scratch wound closure and cell migration in ADSCs

To detect downstream signaling molecules that may be activated by SCF/c-kit, we used gene ontology (GO) analysis to predict possible signaling pathways that regulated by SCF. Then, the top 10 pathway enrichment activated by SCF were displayed in Fig. 6A, such as regulation of cell motility, metabolism response, and mitogen-activated protein kinase (MAPK) cascade. The PPI network was constructed by STRING v.10.5 [25] to predict c-kit-associated proteins (Fig. 6B). During wound healing, tissue regeneration is achieved by activation of crucial signaling pathways. GO and PPI analysis performed on ADSCs upon 24 h of SCF treatment showed enrichment of the MAPK cascade and c-kit associated to ERK, we asked if SCF/c-kit axis triggers the ERK pathway in ADSCs. Firstly, we detected the phosphorylation of ERK in serum-free cultured ADSCs for 6h upon SCF treatment. (0–60 min). As shown in Fig. 6C, increased pERK levels demonstrated that SCF promotes ERK activation in time-dependent manner.

To further determine whether ERK pathway is activated by SCF/c-kit axis, ADSCs transfected with miR-466 mimic were treated with or without ERK inhibitor, PD98059. As shown in Fig. 6D, both mimic and PD98059 treatment inhibited ERK phosphorylation. In addition, mimic and PD98059 impeded ADSCs migration (Fig. 6E, F). Moreover, we use PPI to analyze the possible interaction between ERK and MMPs proteins (Fig. 6G). As shown in Fig. 6H, SCF treatment induced high expression of MMP-2 and MMP-9, but this increase could be blocked by mimic and PD98059.

ERK signal is participated in the auxo-action of miR-466 inhibitor on SCF/c-kit regulated cell migration

Since ERK signal is responsible for the migration of ADSCs activated by SCF/c-kit, we wanted to identify whether miR-466 could influence the activity of ERK induced by SCF/c-kit. From Fig. 7A, we can see that ERK inhibitor, PD98059, treatment resulted in down-regulation of ERK, this was overturned by miR-466 inhibitor. Moreover, miR-466 inhibitor promoted the migration of ADSCs (Fig. 7B, C). The expression of MMP-2 and MMP-9 were also increased by miR-466 inhibitor (Fig. 7D). From the schematic diagram, we infer that miR-466 can suppress migration of ADSCs due to inhibiting SCF/c-kit/ERK (Fig. 7E).

miR-466 inhibits cell migration to wound site and defects cutaneous wound healing in vivo

To determine the power of miR-466 and SCF on cutaneous wound healing in vivo, we used the excisional wound healing mouse model to verify the ability of SCF and miR-466 in tissue repair in vivo. Wounds including the entire dermis and epidermis were created on the back of nu/nu athymic nude mice and were

clamps with silicone rings to limit wound closure caused by skin contraction. We first used DiR marked ADSCs to inject on or into the chronic wounds of mice. As shown in the Fig. 8A, the cells were directly transplanted on the surface of the wound site and there were only a few living cells on the wound site at the 7th day according to in vivo imaging system. Subsequently, DiR marked ADSCs were injected into the mice wound edge and animals were topically and repeatedly treated with SCF in the presence or absence of PD98059 or agonist miR (agomiR). miR-466 agomiR was used to over-expression of miR-466 in the wound site. When the cells were injected into the wound edge, there are more alive cell compared with transplanted on the wound site with living imaging (Fig. 8B). In addition, the topical application of SCF significantly accelerates wound closure on days 7, 14, and 21 compared with ADSCs-treated exhibited complete re-epithelialization. Importantly, PD98059 treatment significantly reduced re-epithelialization compared with SCF and ADSCs-treated mice. Mice treated with SCF and miR-466 agomiR showed slower wound closure than observed in the SCF group at days 7, 14 and 21 post-wounding. H&E staining of the wound site indicated significant increases in the degree of re-epithelialization of the wound after 21 days in the SCF combined with miR-466 agomiR group compared to the SCF group (Fig. 8C, D). Because keratins 10 (K10) is an early marker of cell differentiation into epithelial cell lineage [27], we investigated reveals that the re-epithelialization of K10 was significantly reduced by PD98059 or miR-466 agomiR treated groups (Fig. 8E). The amount of organized and total collagen was significantly greater in SCF-treated wounds compared with the non-treated groups. Importantly, PD98059 and miR-466 reduced the amount of both polarized and total collagen (Fig. 8F). Furthermore, observation of endothelial marker CD31 and αSMA revealed the maturity of blood vessels, indicating the potential of SCF to induce angiogenesis. However, PD98059 and miR-466 impede the maturity of blood vessels (Fig. 8G).

Discussion

Although ADSCs have been shown strong differentiation and secretion ability with significantly improve the activity of fibroblasts, keratinocytes and vascular endothelial cells and accelerating wound healing [28–30], inadequate mobilization ability and low survival rate of transplanted cells lead to limitations of cell therapy [6, 9]. For the sake of safety, stem cells are usually directly inoculated on the wound surface or injected into the wound edge. When inoculated on the wound surface, the cells directly contact with the external environment and often die in large numbers due to inflammation, hypoxia and inadequate nutrition. However, when injected into the wound edge the cell mobilization capacity is insufficient and island-like death of cells tends to occur, but the overall survival rate is still higher. Herein, we demonstrate that ADSCs inject into wound edge had more living cell even at14 days after transplantation with live imaging.

Therefore, we focus on how to accelerate cell mobilization to the wound and expedite wound healing.

Being a chemokine [31], SCF is produced and released by both fibroblasts and endothelial cells, which plays a vital role in attracting stem cells in concentration-manners [32, 33]. For most cells, especially stems cells, SCF and its cognate receptor, c-kit consist an important complex, which regulating their survival and function. Current evidence shows that in diabetic wounded environment the expression of

SCF decreased at some degree [34]. Therefore, a hypothesis formed that exogenous SCF could enhance wound healing by recruiting endo/exo-genous stem cells.

According to our research, SCF/c-kit-induced transcriptional signature is enriched in genes related to wound healing associated biological processes and, specifically, to signaling pathways driving ADSC migration and ERK activation.
Functionally, we testify that incubation of ADSCs with SCF resulted in significant upregulation of c-kit and promoted migration of ADSCs, contributing to angiogenesis and re-epithelialization of wounds. Preliminarily, we discussed that this effect might be related to the increased activity of MMP-2 and MMP-9, which is sustained by ERK activation. In the future, we expect to further apply actinonin (inhibitor of MMPs) to abolish the activity of MMPs and to observe the effect of miR-466/SCF/c-kit/ERK on ADSCs migration.

miRNAs attract researchers' attention as a group of small non-coding single-strand RNAs that control gene expression at the post-transcriptional or translational level by bounding to the 3'UTR of target mRNAs and widely exist in tissue and serum [35]. They can cause degradation or transcription inhibition of mRNA. Researches have demonstrated the involvement of microRNAs (miRNAs) in regulating proliferation and migration of MSCs. For example, miR-9-5p is considered to promote MSC migration by β-catenin signaling pathway [36]. miR-302 is confirmed to induce proliferation of ADSCs decrease oxidative stress [37]. However, only a few studies investigate the role of miRNAs in regulating SCF/c-Kit signaling related to wound healing. Using a miRNA microarray, we surveyed the differential expression of miRNAs after SCF treatment in ADSCs. The results showed that a panel of miRNAs in SCF-treated ADSCs were significantly dysregulated, which may regulate the function of ADSCs under SCF. Therefore, we used TargetScan and miRDB to predict potential miRNAs targeting c-kit. According to these results, we selected miR-466 because it was the only one of up-regulation induced by SCF treatment that was predicted to target c-kit. Subsequently, we revealed that miR-466 could directly bind to the 3'UTR of c-KIT. What's more, miR-466 inhibited the migration of ADSCs via ERK. All findings indicated the vital role of miR-466 in regulating the effect of ADSCs in repairing wound healing via targeting SCF/c-Kit.

MAPK signals can be activated in multiple pathological states. And SCF have been reported to trigger the activation of MAPK cascades in various cell types [38, 39]. It has been shown that SCF/c-Kit complex mediates the migration of CSCs via activation of p38 MAPK [40]. What's more, miRNAs have been identified that modulate MAPK pathway in stem cells. Chen et al find that miR-21 can protect β cells against hypoxia-induced apoptosis by alleviating ER stress and inhibiting p38 MAPK [41]. In addition, miR-125a can attenuate BMSCs apoptosis via the MAPK-ERK pathways in the setting of craniofacial defect reconstruction [42]. To further investigate whether ERK signal is involved in regulating the migration of ADSCs by SCF/c-Kit, we first detected the levels of phosphorylated form of pERK after treated with SCF. We found that ERK pathway is involved in the regulation of migration mediated by SCF/c-kit. Also, we found that SCF/c-kit axis can improve the expression of MMP-2 and MMP-9 by the ERK activation. Then, we detected whether miR-466 can influence the activity of ERK induced by SCF/c-

Kit in ADSCs. Our results showed that miR-466 may inhibit ERK signal activity, which inhibits the migration of ADSCs.

Conclusions

The results of our study highlight the power of SCF treatment to enhance wound healing by promoting migration of ADSCs to wound site. miR-466 can restrain the effect of ADSCs in repairing wound healing via targeting SCF/c-kit axis. Moreover, ERK signal is involved in the auxo-action of miR-466 on SCF/c-kit induced migration of ADSCs. Taken together, our studies provide insights into the mechanism of miR-466 that regulate specifically the effect of ADSCs in repairing wound via targeting SCF/c-kit/ERK signaling in order to formulate improved and optimized miRNA-targeted approaches for accelerating wound healing.

Abbreviations

ADSCs: adipose tissue-derived stem cells; SCF: Stem cell factor; c-kit:stem cell factor receptor; MSC: mesenchymal stem cell; AGEs: advanced glycation end products; mRNAs: messenger RNAs; ERK: extracellular signal regulated kinase; DMEM: L-Dulbecco's modified Eagle's medium; FBS: fetal bovine serum; GO: Gene Ontology; PPI: protein–protein interaction; agomiR: agonist miR; IVIS: in vivo imaging system; DiR: 1,1’-dioctadecyl-3,3,3’,3’-tetramethylindotricarbocyanine; H&E: hematoxylin and eosin; MAPK: mitogen-activated protein kinase.

Declarations

Funding

This work was financially supported by the National key research and development project (2016YFC1100803).

Availability of data and materials

The data that support the findings of this study are available from the corresponding author upon reasonable request.

Acknowledgements

Not applicable.

Authors’ Contributions

C.H., W. X. and S.Z. guided the experimental procedures. R.J., T.W. and W.Z. participated in establishing the experimental animal model. S.Z., M.Y., and S.J. performed the cell culture and biological experiment. S.Z., W.Z., and R.J. performed the performed the animal experiment. S.Z. and R.J. participated in the design of the study and the writing of the manuscript. All authors read and approved the final manuscript.

Ethics approval and consent to participate

This study was conducted under the guidelines and with the approval of the Second Affiliated Hospital of Medical College, Zhejiang University. All patients consented to the respective use of their tissues. All animal experiments were performed at the Animal Center of Zhejiang University and maintained under specific pathogen-free conditions. All animal studies were approved by Animal Care and Use Committee.

Consent for publication

Not applicable.

Competing interests

The authors declare that they have no competing interests.

References

1. Bai Y, Shang Q, Zhao H, Pan Z, Guo C, Zhang L, et al. Pdcd4 restrains the self-renewal and white-to-beige transdifferentiation of adipose-derived stem cells. Cell Death Dis. 2016;7:e2169.
2. Pham-Nguyen OV, Shin JU, Kim H, Yoo HS. Self-assembled cell sheets composed of mesenchymal stem cells and gelatin nanofibers for the treatment of full-thickness wounds. Biomater Sci. 2020;8(16):4535-44.
3. Kang ML, Kim HS, You J, Choi YS, Kwon BJ, Park CH, et al. Hydrogel cross-linking-programmed release of nitric oxide regulates source-dependent angiogenic behaviors of human mesenchymal stem cell. Sci Adv. 2020;6(9):eaay5413.
4. Mazini L, Rochette L, Admou B, Amal S, Malka G. Hopes and Limits of Adipose-Derived Stem Cells (ADSCs) and Mesenchymal Stem Cells (MSCs) in Wound Healing. Int J Mol Sci. 2020;21(4).
5. Luck J, Weil BD, Lowdell M, Mosahebi A. Adipose-Derived Stem Cells for Regenerative Wound Healing Applications: Understanding the Clinical and Regulatory Environment. Aesthet Surg J. 2020;40(7):784-99.
6. Chen L, Zheng Q, Liu Y, Li L, Chen X, Wang L, et al. Adipose-derived stem cells promote diabetic wound healing via the recruitment and differentiation of endothelial progenitor cells into endothelial cells mediated by the VEGF-PLCgamma-ERK pathway. Arch Biochem Biophys. 2020;692:108531.
7. Cai Y, Li J, Jia C, He Y, Deng C. Therapeutic applications of adipose cell-free derivatives: a review. Stem Cell Res Ther. 2020;11(1):312.
8. Lee EY, Xia Y, Kim WS, Kim MH, Kim TH, Kim KJ, et al. Hypoxia-enhanced wound-healing function of adipose-derived stem cells: increase in stem cell proliferation and up-regulation of VEGF and bFGF. Wound Repair Regen. 2009;17(4):540-7.
9. Li Q, Xia S, Yin Y, Guo Y, Chen F, Jin P. miR-5591-5p regulates the effect of ADSCs in repairing diabetic wound via targeting AGEs/AGER/JNK signaling axis. Cell Death Dis. 2018;9(5):566.

10. Schmitt M, Schewe M, Sacchetti A, Feijtel D, van de Geer WS, Teeuwssen M, et al. Paneth Cells Respond to Inflammation and Contribute to Tissue Regeneration by Acquiring Stem-like Features through SCF/c-Kit Signaling. Cell Rep. 2018;24(9):2312-28 e7.
11. Kim JO, Kim HN, Kim KH, Baek EJ, Park JY, Ha K, et al. Development and characterization of a fully human antibody targeting SCF/c-kit signaling. Int J Biol Macromol. 2020;159:66-78.
12. Guan S, Zhu Y, Wang J, Dong L, Zhao Q, Wang L, et al. A combination of Semen Cuscutae and Fructus Lycii improves testicular cell proliferation and inhibits their apoptosis in rats with spermatogenic dysfunction by regulating the SCF/c-kit--PI3K--Bcl-2 pathway. J Ethnopharmacol. 2020;251:112525.
13. Kim KL, Seo S, Kim JT, Kim J, Kim W, Yeo Y, et al. SCF (Stem Cell Factor) and cKIT Modulate Pathological Ocular Neovascularization. Arterioscler Thromb Vasc Biol. 2019;39(10):2120-31.
14. Zgheib C, Xu J, Mallette AC, Caskey RC, Zhang L, Hu J, et al. SCF increases in utero-labeled stem cells migration and improves wound healing. Wound Repair Regen. 2015;23(4):583-90.
15. Li X, Zhang Y, Liang Y, Cui Y, Yeung SC, Ip MS, et al. iPSC-derived mesenchymal stem cells exert SCF-dependent recovery of cigarette smoke-induced apoptosis/proliferation imbalance in airway cells. J Cell Mol Med. 2017;21(2):265-77.
16. Lam CR, Tan MJ, Tan SH, Tang MB, Cheung PC, Tan NS. TAK1 regulates SCF expression to modulate PKBalpha activity that protects keratinocytes from ROS-induced apoptosis. Cell Death Differ. 2011;18(7):1120-9.
17. Mukhopadhyay A, Do DV, Ong CT, Khoo YT, Masilamani J, Chan SY, et al. The role of stem cell factor and c-KIT in keloid pathogenesis: do tyrosine kinase inhibitors have a potential therapeutic role? Br J Dermatol. 2011;164(2):372-86.
18. Niwano T, Terazawa S, Nakajima H, Imokawa G. The stem cell factor-stimulated melanogenesis in human melanocytes can be abrogated by interrupting the phosphorylation of MSK1: evidence for involvement of the p38/MSK1/CREB/MITF axis. Arch Dermatol Res. 2018;310(3):187-96.
19. Wang Y, Li J, Kuang D, Wang X, Zhu Y, Xu S, et al. miR-148b-3p functions as a tumor suppressor in GISTs by directly targeting KIT. Cell Commun Signal. 2018;16(1):16.
20. Zhao Y, Ransom JF, Li A, Vedantham V, von Drehle M, Muth AN, et al. Dysregulation of cardiogenesis, cardiac conduction, and cell cycle in mice lacking miRNA-1-2. Cell. 2007;129(2):303-17.
21. Rottiers V, Naar AM. MicroRNAs in metabolism and metabolic disorders. Nat Rev Mol Cell Biol. 2012;13(4):239-50.
22. Singh SK, Pal Bhadra M, Girschick HJ, Bhadra U. MicroRNAs--micro in size but macro in function. FEBS J. 2008;275(20):4929-44.
23. Hu Y, Rao SS, Wang ZX, Cao J, Tan YJ, Luo J, et al. Exosomes from human umbilical cord blood accelerate cutaneous wound healing through miR-21-3p-mediated promotion of angiogenesis and fibroblast function. Theranostics. 2018;8(1):169-84.
24. Wang W, Yang C, Wang XY, Zhou LY, Lao GJ, Liu D, et al. MicroRNA-129 and -335 Promote Diabetic Wound Healing by Inhibiting Sp1-Mediated MMP-9 Expression. Diabetes. 2018;67(8):1627-38.

25. Szklarczyk D, Morris JH, Cook H, Kuhn M, Wyder S, Simonovic M, et al. The STRING database in 2017: quality-controlled protein-protein association networks, made broadly accessible. Nucleic Acids Res. 2017;45(D1):D362-D8.
26. Yan Y, Wu R, Bo Y, Zhang M, Chen Y, Wang X, et al. Induced pluripotent stem cells-derived microvesicles accelerate deep second-degree burn wound healing in mice through miR-16-5p-mediated promotion of keratinocytes migration. Theranostics. 2020;10(22):9970-83.
27. Sporl F, Wunderskirchner M, Ullrich O, Bomke G, Breitenbach U, Blatt T, et al. Real-time monitoring of membrane cholesterol reveals new insights into epidermal differentiation. The Journal of investigative dermatology. 2010;130(5):1268-78.
28. Niu Y, Chen Y, Xu H, Wang Q, Xue C, Zhu R, et al. Astragaloside IV Promotes Antiphotoaging by Enhancing the Proliferation and Paracrine Activity of Adipose-Derived Stem Cells. Stem Cells Dev. 2020;29(19):1285-93.
29. Pu CM, Liu CW, Liang CJ, Yen YH, Chen SH, Jiang-Shieh YF, et al. Adipose-Derived Stem Cells Protect Skin Flaps against Ischemia/Reperfusion Injury via IL-6 Expression. J Invest Dermatol. 2017;137(6):1353-62.
30. Ong HT, Redmond SL, Marano RJ, Atlas MD, von Unge M, Aabel P, et al. Paracrine Activity from Adipose-Derived Stem Cells on In Vitro Wound Healing in Human Tympanic Membrane Keratinocytes. Stem Cells Dev. 2017;26(6):405-18.
31. Asada N, Kunisaki Y, Pierce H, Wang Z, Fernandez NF, Birbrair A, et al. Differential cytokine contributions of perivascular haematopoietic stem cell niches. Nat Cell Biol. 2017;19(3):214-23.
32. Shen SQ, Wang R, Huang SG. Expression of the stem cell factor in fibroblasts, endothelial cells, and macrophages in periapical tissues in human chronic periapical diseases. Genet Mol Res. 2017;16(1).
33. Liao CP, Booker RC, Brosseau JP, Chen Z, Mo J, Tchegnon E, et al. Contributions of inflammation and tumor microenvironment to neurofibroma tumorigenesis. J Clin Invest. 2018;128(7):2848-61.
34. Jin QH, Shen HX, Wang H, Shou QY, Liu Q. Curcumin improves expression of SCF/c-kit through attenuating oxidative stress and NF-kappaB activation in gastric tissues of diabetic gastroparesis rats. Diabetol Metab Syndr. 2013;5(1):12.
35. Thomou T, Mori MA, Dreyfuss JM, Konishi M, Sakaguchi M, Wolfrum C, et al. Adipose-derived circulating miRNAs regulate gene expression in other tissues. Nature. 2017;542(7642):450-5.
36. Li X, He L, Yue Q, Lu J, Kang N, Xu X, et al. MiR-9-5p promotes MSC migration by activating beta-catenin signaling pathway. Am J Physiol Cell Physiol. 2017;313(1):C80-C93.
37. Kim JY, Shin KK, Lee AL, Kim YS, Park HJ, Park YK, et al. MicroRNA-302 induces proliferation and inhibits oxidant-induced cell death in human adipose tissue-derived mesenchymal stem cells. Cell Death Dis. 2014;5:e1385.
38. MacNeil AJ, Junkins RD, Wu Z, Lin TJ. Stem cell factor induces AP-1-dependent mast cell IL-6 production via MAPK kinase 3 activity. J Leukoc Biol. 2014;95(6):903-15.
39. Benson DM, Jr., Yu J, Becknell B, Wei M, Freud AG, Ferketich AK, et al. Stem cell factor and interleukin-2/15 combine to enhance MAPK-mediated proliferation of human natural killer cells.

Blood. 2009;113(12):2706-14.

40. Kuang D, Zhao X, Xiao G, Ni J, Feng Y, Wu R, et al. Stem cell factor/c-kit signaling mediated cardiac stem cell migration via activation of p38 MAPK. Basic Res Cardiol. 2008;103(3):265-73.
41. Chen J, Chen J, Cheng Y, Fu Y, Zhao H, Tang M, et al. Mesenchymal stem cell-derived exosomes protect beta cells against hypoxia-induced apoptosis via miR-21 by alleviating ER stress and inhibiting p38 MAPK phosphorylation. Stem Cell Res Ther. 2020;11(1):97.
42. Fan L, Wang J, Ma C. miR125a attenuates BMSCs apoptosis via the MAPK-ERK pathways in the setting of craniofacial defect reconstruction. J Cell Physiol. 2020;235(3):2857-65.

Figures

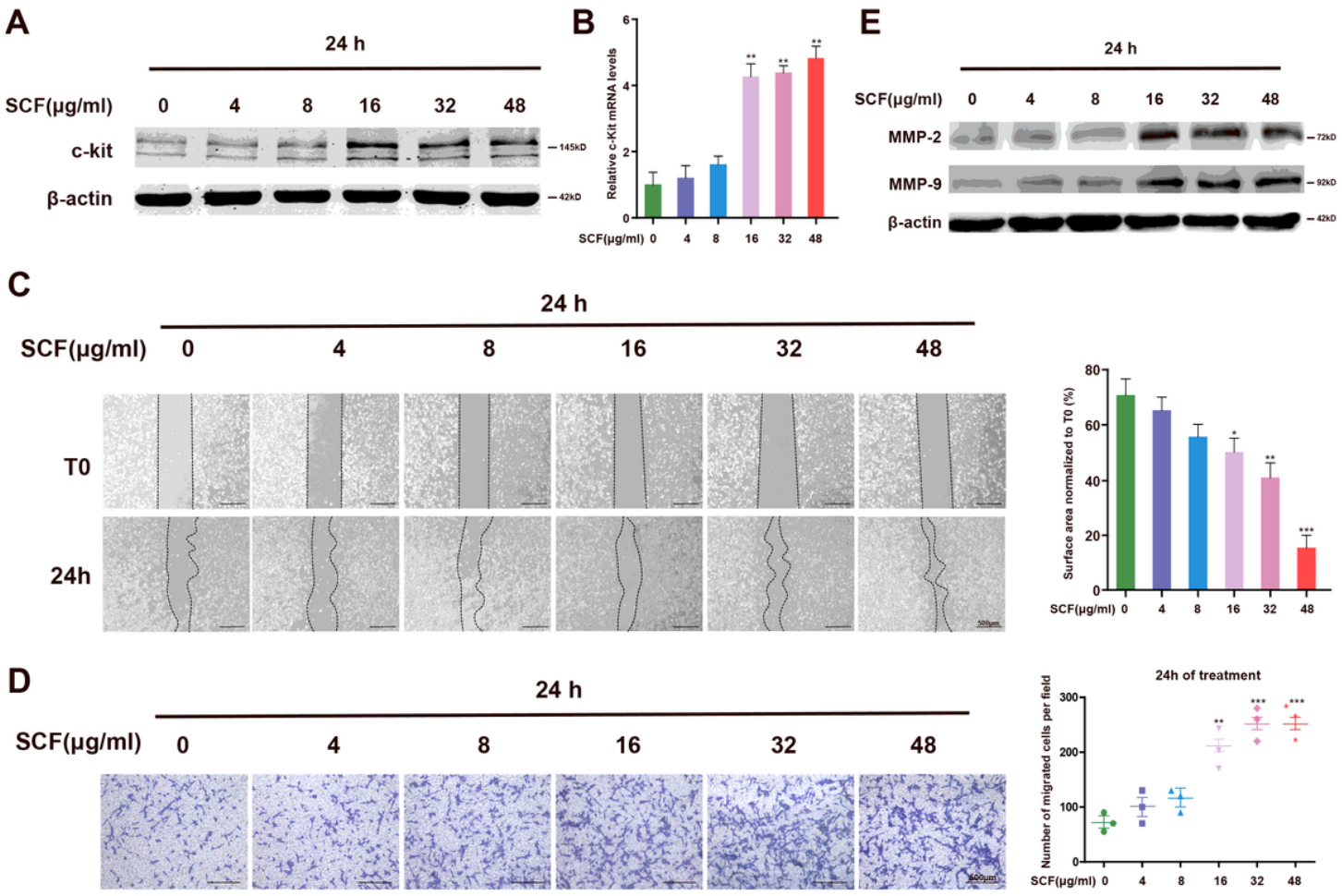

Figure 1

Different concentration of SCF on expression of c-kit, scratch wound closure and migration in ADSCs. A. Representative Western blot images showing the protein expression levels of c-kit when ADSCs treated with different concentration of SCF. B. RT-qPCR analysis of mRNA levels of c-kit after cells treated with different concentration of SCF. C. Representative images and quantification SCF-treated (24 h) and untreated ADSCs in a scratch wound assay. SCF was applied for different concentration periods (4, 8, 12,

32 and 48 μg/ml). Scratch wound closure percentage was observed under light microscope and analyzed using ImageJ software. Scale bar=500μm. D. Microscopic observation of untreated and SCF-treated transwell chambers. Migrated cells were stained with crystal violet (0.1%), observed under a light microscope and analyzed using ImageJ software. Scale bar=500μm E. Western blot analysis of protein levels of MMP-2 and MMP-9. Every experiment repeated at least three times. Error bars indicate mean ± SD (*P<0.05, **P<0.01 and ***P<0.001).

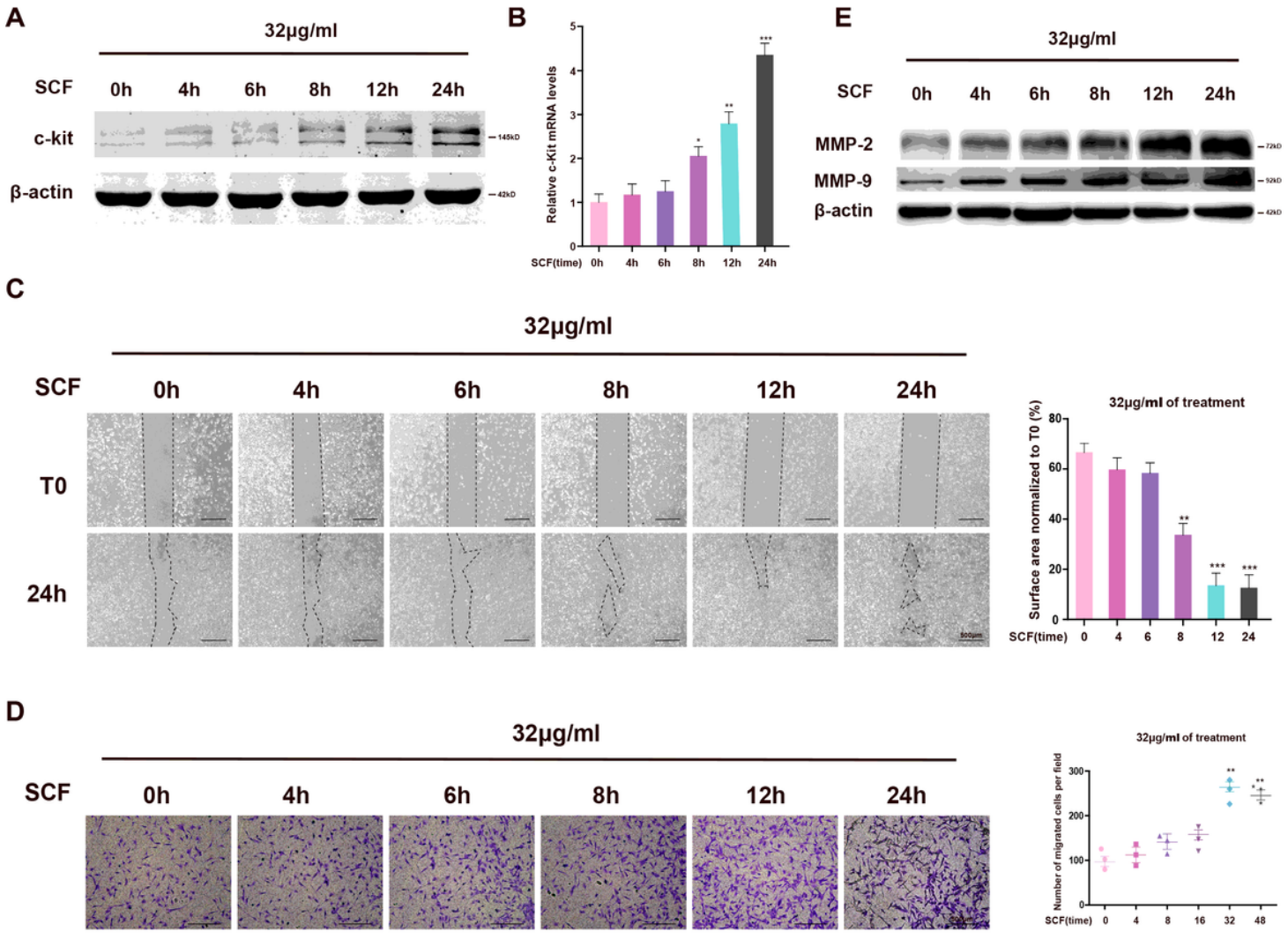

Figure 2

Time course of SCF on expression of c-kit, scratch wound closure and migration in ADSCs. A. Representative Western blot images showing time course of c-kit protein expression in ADSCs treated with SCF (32 μg/ml). B. qRT-PCR analysis of mRNA levels of c-kit after cells treated with different time of SCF. C. Representative images and quantification SCF-treated and untreated ADSCs in a scratch wound assay. SCF was applied for different time periods (4, 6, 8, 12 and 24 h). Scratch wound closure percentage was observed under light microscope and analyzed using ImageJ software. Scale bar=500μm. D. Microscopic observation of untreated and SCF-treated transwell chambers. Scale

bar=500μm E. Western blot analysis of protein levels of MMP-2 and MMP-9. Every experiment repeated at least three times. Error bars indicate mean ± SD (*P<0.05, **P<0.01 and ***P<0.001).

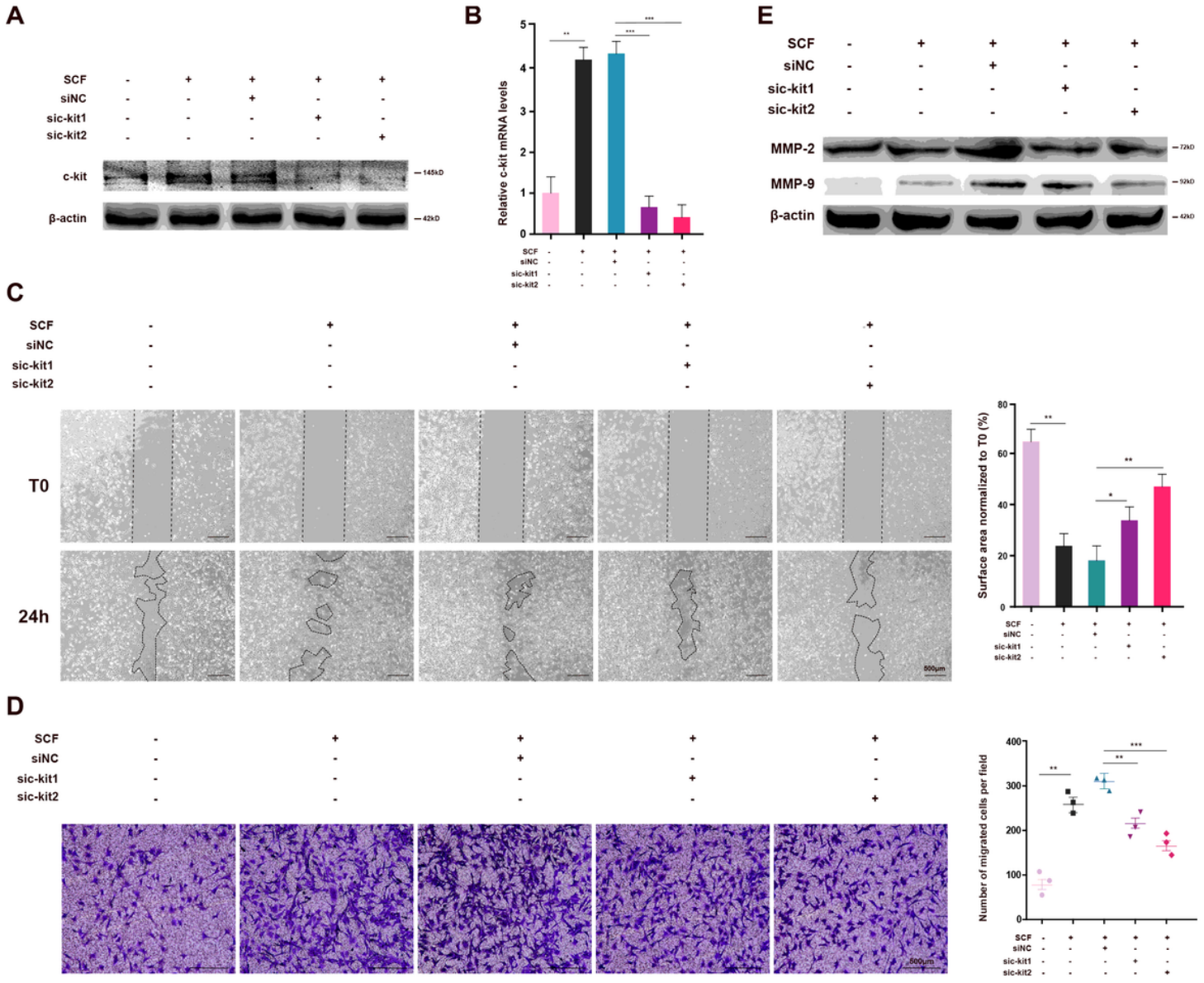

Figure 3

The effect of siRNA c-kit on scratch wound closure and migration in ADSCs. A. Western blot shows the protein expression of c-kit after transfect with siRNAs for c-kit in ADSCs. β-actin was used as an internal control. B. RT-qPCR analysis of mRNA levels of c-kit after cells were transfected with siRNAs for c-kit. GAPDH was used as an internal control. C. Representative images and quantification siRNAs for c-kit transfect in ADSCs in a scratch wound assay. Scale bar=500μm. D. Microscopic observation of siRNAs for c-kit transfect transwell chambers. Scale bar=500μm. E. Western blot analysis of protein levels of MMP-2 and MMP-9. Every experiment repeated at least three times. Error bars indicate mean ± SD (*P<0.05, **P<0.01 and ***P<0.001).

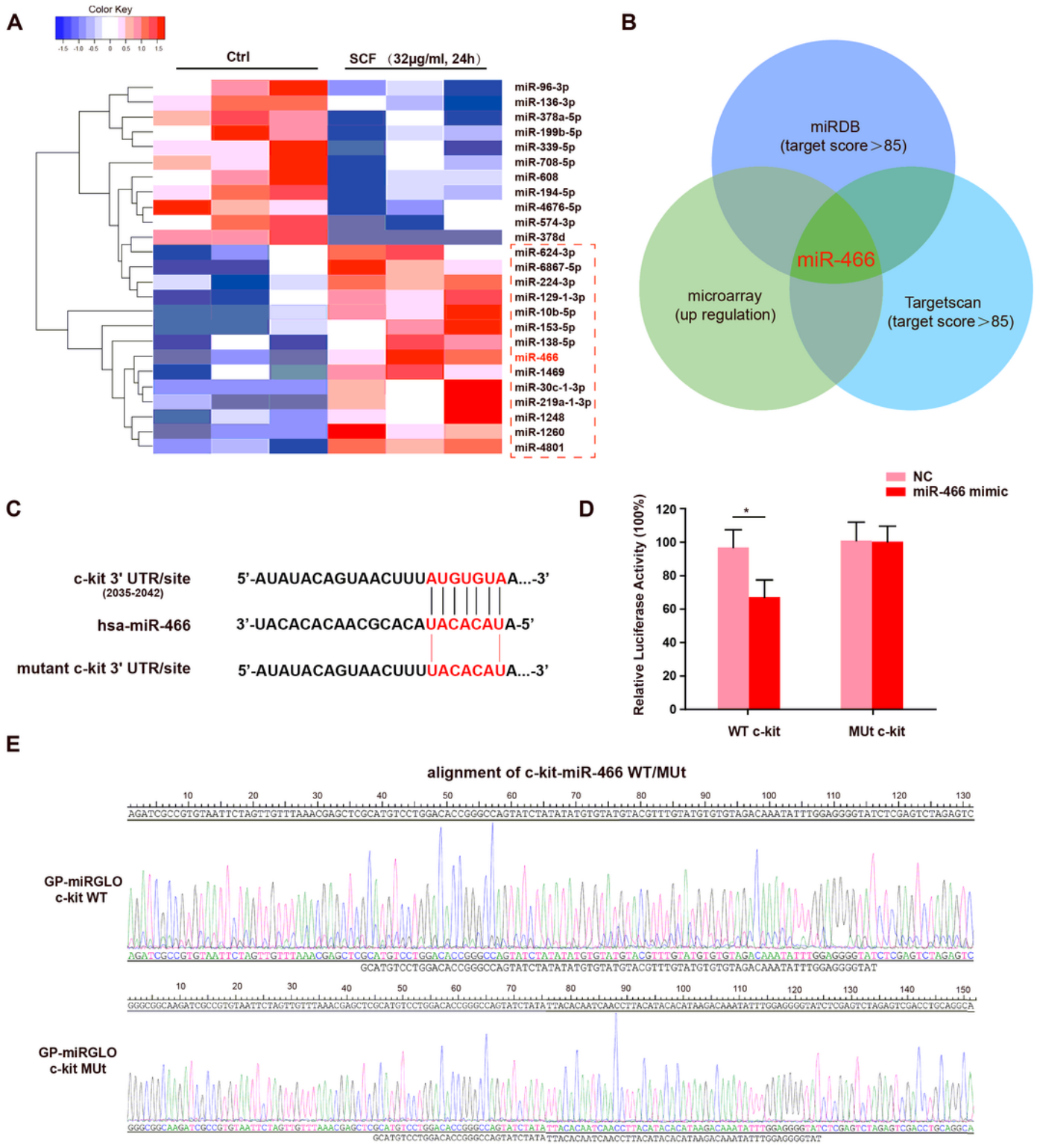

Figure 4

c-kit is a target of miR-466. A. miRNAs microarray showing differentially expressed miRNAs in ADSCs treated with or without SCF. A color scale is shown on the top of the heat map. B. The predicted site of miR-466 binding to the c-kit 3'-UTR were detected based on bioinformatics and miRNAs Microarray results. C. The binding sites of wild type (WT) and mutant type (MUT) of c-kit 3'-UTR are shown. D. The dual luciferase reporter gene demonstrated the effect of miR-466 binding to GP-miRGLO-c-kit-WT and GP-

miRGLO-c-kit-MUT reporter plasmids in ADSCs. E. The alignment of c-kit-miR-466 WT/Mut. Error bars indicate mean ± SD (*P<0.05).

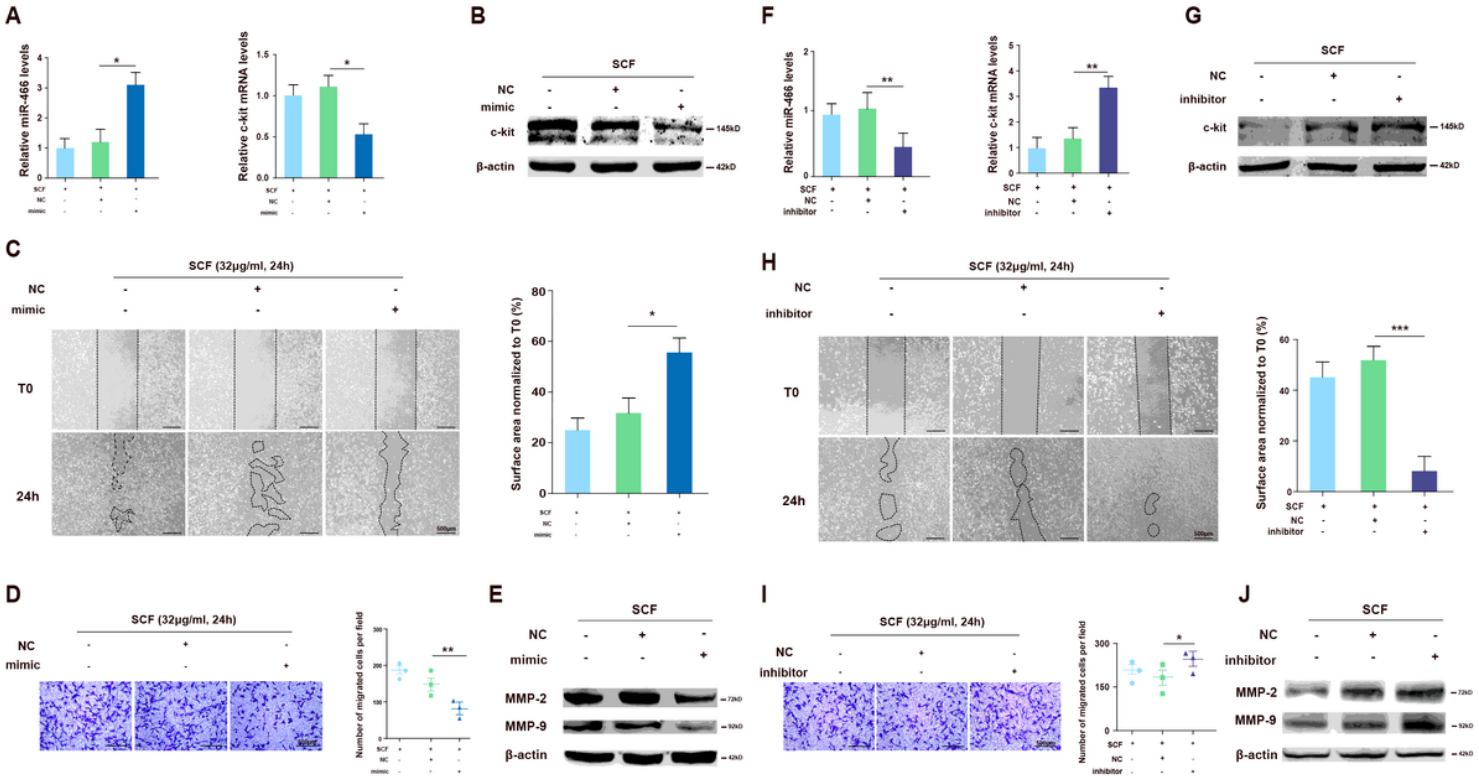

Figure 5

miR-466 suppresses SCF/c-kit axis-mediated scratch wound closure and migration in ADSCs. A. RT-qPCR analysis of mRNA levels of c-kit and miR-466 after cells were transfected miR-466 mimic with SCF pretreated. B. Western blot shows protein levels of c-kit after cells were transfected miR-466 mimic with SCF pretreated. C. Representative images and quantification miR-466 mimic transfect in ADSCs in a scratch wound assay with SCF pretreated. Scale bar=500μm. D. Microscopic observation of miR-466 mimic transfect transwell chambers with SCF pretreated in ADSCs. Scale bar=500μm. E. Western blot analysis of protein levels of MMP-2 and MMP-9. F. RT-qPCR analysis of mRNA levels of c-kit and miR-466 after cells were transfected miR-466 inhibitor with SCF pretreated. G. Western blot shows protein levels of c-kit after cells were transfected miR-466 inhibitor with SCF pretreated. H. Representative images and quantification miR-466 inhibitor transfect in ADSCs in a scratch wound assay with SCF pretreated. Scale bar=500μm. I. Microscopic observation of miR-466 inhibitor transfect transwell chambers with SCF pretreated in ADSCs. Scale bar=500μm. J. Western blot analysis of protein levels of MMP-2 and MMP-9. Every experiment repeated at least three times. Error bars indicate mean ± SD (*P<0.05, **P<0.01 and ***P<0.001).

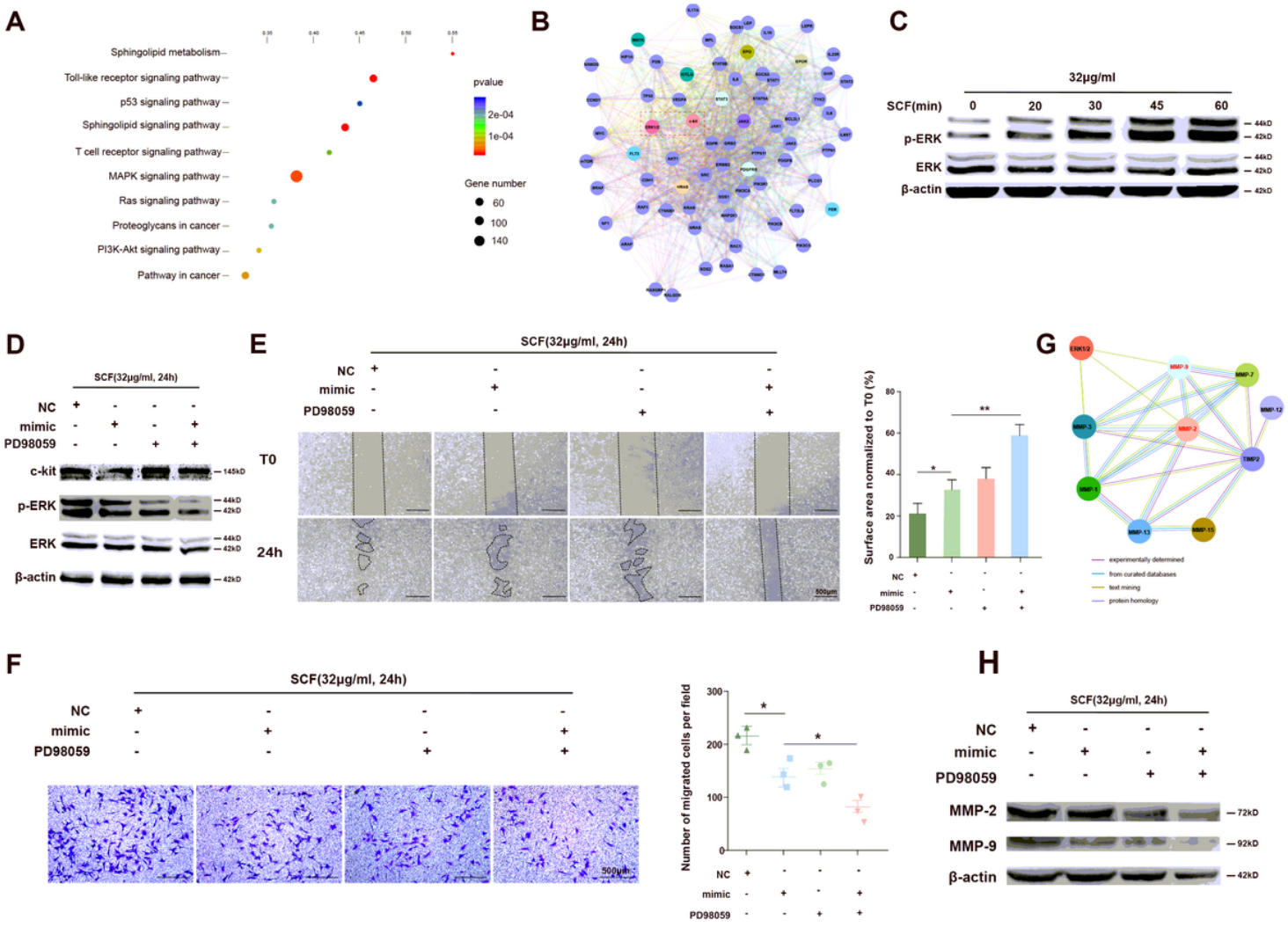

Figure 6

Role of ERK signal in SCF/c-kit induced scratch wound closure and migration in ADSCs. A. Enrichment analysis of the signal pathway exhibited the top 10 intracellular signal transduction types in which SCF may be involved. A color scale is shown on the right. B. The Protein–Protein Interaction Network (PPI) analyzed proteins that might interact with c-kit with the STRING repository. C. Western blot shows time course of phosphorylated and total ERK protein expression in ADSCs (serum-free cultured with 6 h) treated with SCF (32 μg/ml). D. ADSCs pretreated with SCF were transfected with miR-466 mimic and ERK inhibitor, PD98059. The protein levels of phosphorylated and total ERK, c-kit and β-actin were determined by Western blot analysis. E. Representative images and quantification of mimic transfected in ADSCs in a scratch wound assay with or without PD98059 pretreated. Scale bar=500μm. F. Microscopic observation of mimic transfect in ADSCs in a transwell assay with or without PD98059 pretreated. Scale bar=500μm. G. PPI analyzed proteins that might interact with ERK with the STRING repository. H. Western blot analysis of protein levels of MMP-2 and MMP-9. Every experiment repeated at least three times. Error bars indicate mean ± SD (*P<0.05 and **P<0.01).

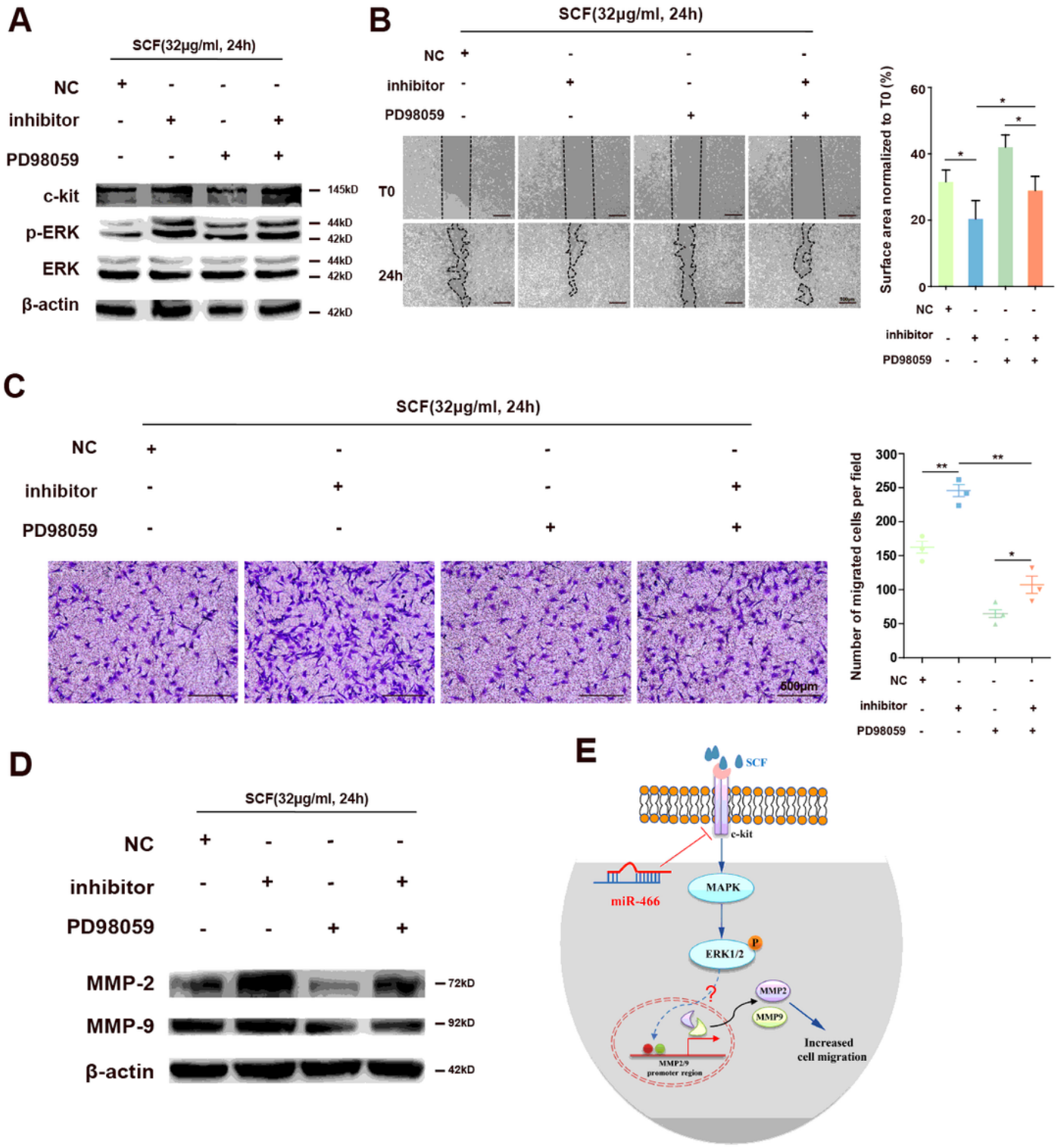

Figure 7

Effect of ERK on scratch wound closure and migration induced by miR-466/SCF/c-kit in ADSCs. A. ADSCs pretreated with SCF were transfected with miR-466 inhibitor and PD98059. The protein levels of phosphorylated and total ERK, c-kit and β-actin were determined by Western blot analysis. B. Representative images and quantification of miR-466 inhibitor transfected in ADSCs in a scratch wound assay with or without PD98059 pretreated. Scale bar=500μm. C. Microscopic observation of miR-466

inhibitor transfected in ADSCs in a transwell assay with or without PD98059 pretreated. Scale bar=500μm. D. Western blot analysis of protein levels of MMP-2 and MMP-9. E. Schematic diagram of miR-466 regulates migration via SCF/c-kit/ERK signaling axis. We infer that miR-466 can suppress migration of ADSCs due to inhibiting SCF/c-kit/ERK pathway by direct target c-kit. Every experiment repeated at least three times. Error bars indicate mean ± SD (*P<0.05 and **P<0.01).

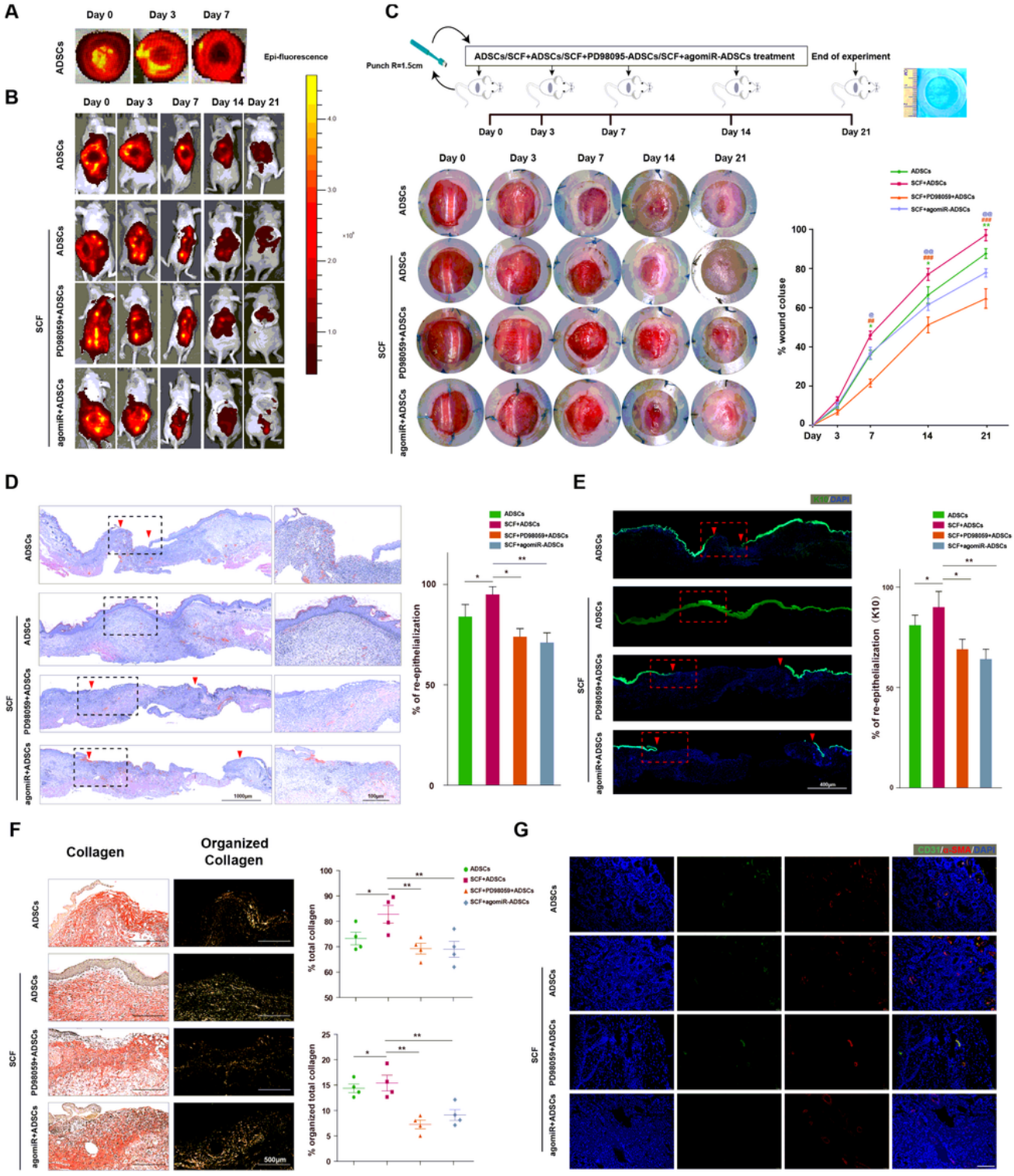

Figure 8

miR-466 inhibits transplanted cell viability and hinders cutaneous wound healing of nude mice. A. In vivo imaging system was used to detect DiR fluorescence after DiR marked ADSCs, which were transplanted on the surface of excisional wounds in 0, 3 and 7 day, respectively. B. In vivo imaging system was used to detect DiR fluorescence after DiR marked ADSCs (SCF, PD98059 and agomiR), which were injected into the skin around excisional wounds in 0, 3, 7, 14 and 21 day, respectively. A color scale is shown on the right. C. Above: schematic representation of the in vivo wound healing research on nude mice. At the end of the experiment (day 21), skin wound samples were collected for further analyses. Below: Excisional wound-splinting assay showing SCF pretreated ADSCs have better ability to improve wound closure compared with the other conditions under study (PD98059 and agomiR). Percentage of wound closure between the groups under study. D. Representative hematoxylin and eosin (H&E) stained section on day 21 after wounding. Pink dotted lines delimitate the epithelial tongues and 10× zoomed region of interest is reported on the right. Scale bar=1000μm. E. Representative immunofluorescence staining showed the expression and position of K10 in the skin on day 21 after wounding. Red Arrowheads delimitate the epithelial tongues of K10 and percentage of re-epithelialization (K10) expressed in arbitrary units among the evaluated groups on the right. Scale bar=400μm. F. Left: representative Sirius Red (SR) stained section on day 21 after wounding. Right: percentage of total collagen formation and percentage organized collagen on the total collagen was evaluated between the conditions. Scale bar=100μm.G. Representative immunofluorescence on day 21 after wounding showing presence of CD31 + and □-SMA + vessels. Scale bar=100μm. (*P<0.05; **P<0.01; *P vs ADSCs, #P vs PD98059 and @P vs agomiR)